

Observation of a Threshold Cusp at the $\Lambda\eta$ Threshold in the pK^- Mass Spectrum with $\Lambda_c^+ \rightarrow pK^-\pi^+$ Decays

(The Belle Collaboration)

We observe a narrow peaking structure in the pK^- invariant-mass spectrum near the $\Lambda\eta$ threshold. The peak is clearly seen in 1.5 million events of $\Lambda_c^+ \rightarrow pK^-\pi^+$ decay using the 980 fb^{-1} data sample collected by the Belle detector at the KEKB asymmetric-energy e^+e^- collider. We try two approaches to explain this structure: as a new resonance and as a cusp at the $\Lambda\eta$ threshold. The best fit is obtained with a coherent sum of a Flatté function and a constant background amplitude with the $\chi^2/\text{n.d.f} = 257/243$ ($p = 0.25$), while the fits to Breit-Wigner functions are disfavored by more than 7σ . The best fit explains the structure as a cusp at the $\Lambda\eta$ threshold and the obtained parameters are consistent with the known properties of $\Lambda(1670)$. The observation gives the first identification of a threshold cusp in hadrons from the spectrum shape.

Regions around the mass thresholds of two hadrons have been of great interest for studies of exotic hadrons such as $X(3872)$ and $P_c(4312)^+$ [1–3], which are found near mass thresholds of two hadrons. These near-threshold resonances could appear as threshold cusps instead of usual smooth peaks with Breit-Wigner (BW) shape. A cusp, defined as a discontinuity in the derivative of spectrum function, always appears exactly at the threshold, and its position does not reflect the pole position of a resonance [4]. To understand the nature of a near threshold behavior, it is necessary to identify whether the peak structure is a threshold cusp or usual peak of BW type. In principle, a threshold cusp can be distinguished from a smooth peak because the derivative diverges at the peak position, but practically, experimental mass resolution often makes such identification difficult [5]. Therefore, there are just a few cases where threshold cusp is identified [6–10], and none of them are from the spectrum shape.

In this Letter, we report a newly discovered peaking structure in the pK^- mass spectrum near the $\Lambda\eta$ mass threshold [11]. A trace of this peak structure is observed in the previous

analysis [12] of $\Lambda_c^+ \rightarrow pK^-\pi^+$ decay using a 980 fb^{-1} data sample collected by the Belle Collaboration. A similar structure is also seen by LHCb in the same Λ_c^+ decay channel [13]. We approach this peak considering two possible cases; a BW-type peak and a visible $\Lambda\eta$ threshold cusp enhanced by the $\Lambda(1670)$ pole nearby.

If it is a BW-type peak, it suggests an existence of a new resonance. In this regard, two theory groups independently proposed a narrow Λ^* resonance with spin $3/2$ near the $\Lambda\eta$ threshold [14, 15] based on the $pK^- \rightarrow \Lambda\eta$ data [16], and the peak could be due to this Λ^* resonance in the $\Lambda_c^+ \rightarrow pK^-\pi^+$ decay as shown in Fig. 1(a). Such an exotic state is not expected in the quark model, and thus it is important to study the observed peak structure to see whether it is the case or not.

On the other hand, a visible cusp can arise via the $\Lambda\eta$ rescattering process in the $\Lambda_c^+ \rightarrow pK^-\pi^+$ decay as shown in Fig. 1(b). In this case, the $\Lambda(1670)$ could be involved in the S -wave $\eta\Lambda$ - pK^- rescattering. Therefore, the shape of the peaking structure is determined by the properties of $\Lambda(1670)$ such as partial widths of the $\Lambda(1670)$ into pK^- and $\eta\Lambda$ channels.

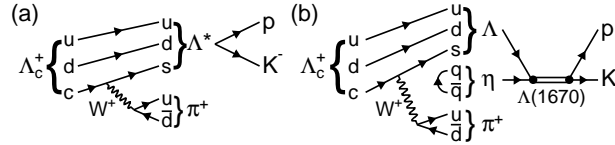


FIG. 1. Feynman diagrams for (a) a new Λ^* resonance and (b) a visible $\Lambda\eta$ threshold cusp enhanced by the $\Lambda(1670)$ pole in $\Lambda_c^+ \rightarrow pK^-\pi^+$ decay.

In this analysis, we use data collected by the Belle detector at the KEKB asymmetric-energy e^+e^- collider [17]. The data sample is taken at or near the $\Upsilon(nS)$ ($n=1-5$) resonances. The Belle detector is a large-solid-angle magnetic spectrometer consisting of a silicon vertex detector (SVD) [18], a central drift chamber (CDC), an array of aerogel threshold Cherenkov counters (ACC), barrel-like arrangement of time-of-flight scintillation counters (TOF), and an electromagnetic calorimeter composed of CsI(Tl) crystals (ECL) located inside a superconducting solenoid coil with a 1.5 T magnetic field. The detector is described in detail elsewhere [19].

We also use samples of $e^+e^- \rightarrow c\bar{c}$ Monte Carlo (MC) events to estimate reconstruction efficiencies and detector performance. The MC simulation samples are generated with PYTHIA [20] and EVTGEN [21] and propagated by GEANT3 [22].

The same event selection criteria as in the previous $\Lambda_c^+ \rightarrow pK^-\pi^+$ analysis [12] are used to reconstruct the decay event from the charged p , K^- , and π^+ . All charged tracks have a distance-of-closest-approach to the interaction point of less than 2.0 cm in the beam direction (z) and less than 0.2 cm in the transverse (r - ϕ) direction. They are also required at least one SVD hit. The particle identification (PID) likelihoods $\mathcal{L}(h)$ (h is p^\pm , K^\pm , or π^\pm) are derived from measurements using the CDC, TOF, and ACC [23]. The ratio of likelihoods, $\mathcal{R}(h : h')$, is defined as $\mathcal{L}(h)/[\mathcal{L}(h) + \mathcal{L}(h')]$ for h and h' identification. The PID requirements for the three charged hadrons are $\mathcal{R}(p : K) > 0.9$ and $\mathcal{R}(p : \pi) > 0.9$ for p , $\mathcal{R}(K : p) > 0.4$ and $\mathcal{R}(K : \pi) > 0.9$ for K^- , and $\mathcal{R}(\pi : p) > 0.4$ and $\mathcal{R}(\pi : K) > 0.4$ for π^+ . In addition, the electron likelihood ratio derived from ACC, CDC, and ECL measurements is required to be less than 0.9 for all hadrons [24]. To reduce combinatorial backgrounds, we require a scaled momentum, defined as $p^*/\sqrt{E_{\text{cm}}^2/4 - M^2}$, to be greater than 0.53; here, p^* , E_{cm} , and M are the Λ_c^+ momentum in the center of mass frame, the total center-of-mass energy, and the mass of the Λ_c^+ candidate, respectively. The three charged tracks are fitted to a common vertex, and the χ^2 value of the vertex fit is required to be less than 40. The 1.5×10^6 $\Lambda_c^+ \rightarrow pK^-\pi^+$ decays are reconstructed with these event selection criteria. For removing non- Λ_c^+ backgrounds, we subtract events in the signal range, $2.2746 < M(pK^-\pi^+) < 2.2986$ GeV/ c^2 , by events in the sideband ranges, $2.2506 < M(pK^-\pi^+) < 2.2626$ GeV/ c^2 and $2.3106 < M(pK^-\pi^+) < 2.3226$ GeV/ c^2 .

To improve the invariant-mass resolution on the $M(pK^-)$ distribution, three daughter particles of the decay are fitted to the common vertex point with the mass of Λ_c^+ . After this mass-constraint vertex fit, detector responses at 1663.5 MeV/ c^2 on the $M(pK^-)$ distribution can be represented by a double-Gaussian function with a common central mean value. From a MC simulation, standard deviations of the core and tail Gaussian functions are determined to be 1.25 MeV/ c^2 and 2.50 MeV/ c^2 , respectively, and the yield of the tail Gaussian function is 0.193 of the core Gaussian function.

We estimate the reconstruction efficiency of $\Lambda_c^+ \rightarrow pK^-\pi^+$ decay using the MC sample. Due to variations of the estimated efficiencies on $M^2(K^-\pi^+)$ and $M(pK^-)$, we correct the Λ_c^+ yields in individual bins of the two-dimensional distribution of $M^2(K^-\pi^+)$ versus $M(pK^-)$.

From the perspective of the pK^- peak as a usual hadron resonance structure, we perform a binned least- χ^2 fit to the efficiency-corrected $M(pK^-)$ distribution in the range of 1.54

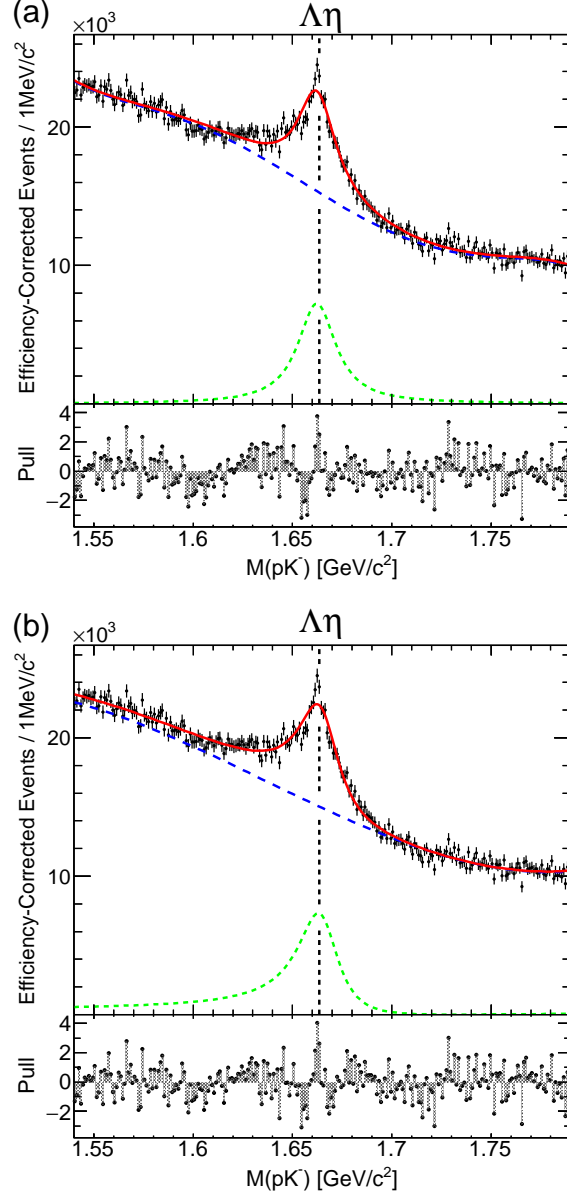


FIG. 2. Fits to the Λ_c^+ yield in $M(pK^-)$ spectra with (a) BW function and (b) BW model to which a complex constant is added. The curves indicate the full fit model (solid red), background Λ_c^+ decay events (long-dashed blue), (a) BW peak (dashed green), and (b) BW model with complex constant added coherently (dashed green). The $\Lambda\eta$ threshold is marked by the vertical dashed lines. The bottom panels show the pull distributions of the fits.

GeV/c^2 to $1.79 \text{ GeV}/c^2$ with a non-relativistic BW function defined as

$$\frac{dN}{dm} \propto |\text{BW}(m)|^2 = \left| \frac{1}{(m - m_0) + i\frac{\Gamma_0}{2}} \right|^2, \quad (1)$$

where m , m_0 , and Γ_0 are the pK^- invariant mass, the nominal mass, and the resonance width, respectively [25]. The BW function is convolved with the double-Gaussian function with fixed parameters to take into account detector responses. The probability density function (PDF) for background Λ_c^+ decay events is a fifth-order Chebyshev polynomial function. Figure 2(a) shows the fit results using the BW function. The mass and width are obtained to be 1662.4 ± 0.3 MeV/ c^2 and 22.6 ± 1.5 MeV, respectively, where the uncertainties are statistical. The reduced χ^2 is 1.35 (328/242).

A better reduced χ^2 is obtained by adding a complex constant to the non-relativistic BW function coherently as $\frac{dN}{dm} \propto |\text{BW}(m) + re^{i\theta}|^2$, where r and θ are real parameters, and θ is fixed to π , leading to constructive interference below the $\Lambda\eta$ threshold and destructive above that. Incoherent background Λ_c^+ decay events are represented by a third-order Chebyshev polynomial. Figure 2(b) shows the fit results including the interference and the mass and width are obtained as 1665.4 ± 0.5 MeV/ c^2 and 23.8 ± 1.2 MeV, respectively, where the uncertainties are only statistical, with the reduced χ^2 of 1.27 (308/243).

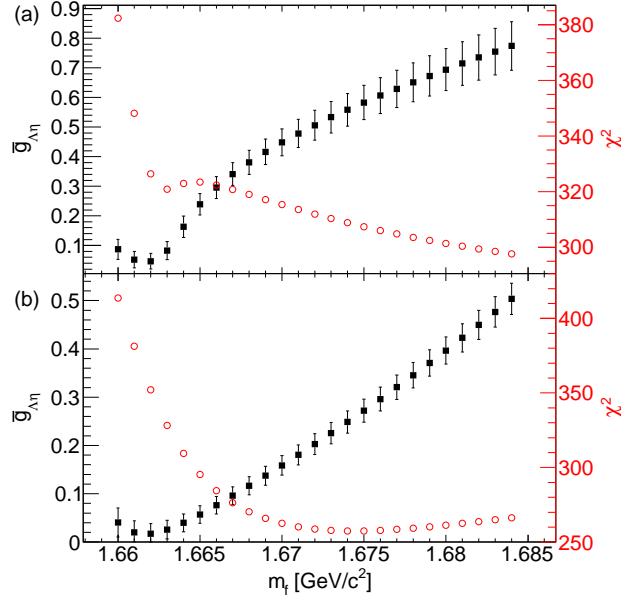


FIG. 3. $\bar{g}_{\Lambda\eta}$ and χ^2 from Flatté model (a) without and (b) with the interference as a function of fixed m_f . The black square and red circle markers indicate $\bar{g}_{\Lambda\eta}$ and χ^2 , respectively. Number of degree of freedom is 242 for all fits in (a) and 243 for all fits in (b). Uncertainty of $\bar{g}_{\Lambda\eta}$ is statistical.

Another possibility is that the peak structure is a cusp at the $\Lambda\eta$ threshold enhanced by

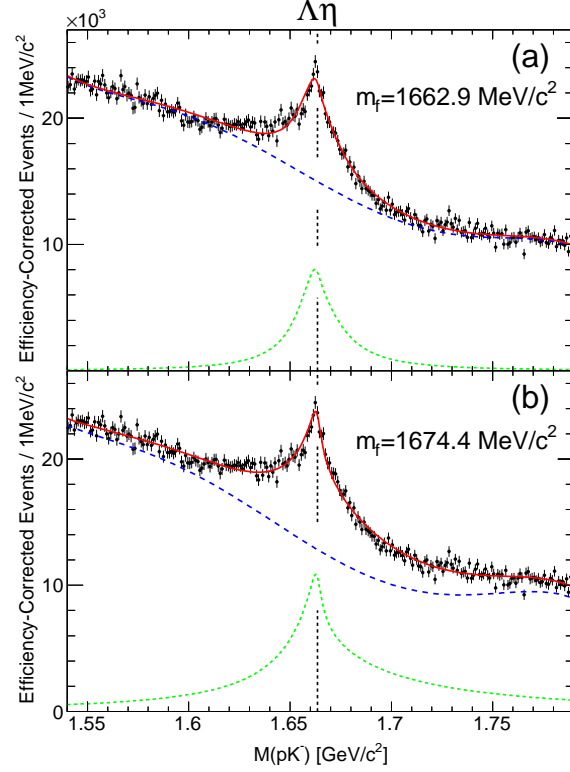


FIG. 4. Fits with Flatté function when m_f is fixed to (a) 1662.9 MeV/ c^2 and (b) 1674.4 MeV/ c^2 . The curves indicate the full fit model (solid red), Flatté function (dashed green), and background Λ_c^+ decay events (long-dashed blue).

the $\Lambda(1670)$ pole nearby. We fit a non-relativistic Flatté function [26, 27] defined as

$$\frac{dN}{dm} \propto |f(m)|^2 = \left| \frac{1}{m - m_f + \frac{i}{2}(\Gamma' + \bar{g}_{\Lambda\eta}k)} \right|^2, \quad (2)$$

to the peak region, where m is the pK^- invariant mass and m_f is a parameter corresponding to the nominal mass of $\Lambda(1670)$. The Γ' is a parameter for the sum of the partial widths of the decay modes other than $\Lambda\eta$, and is approximated as a constant in the following analysis. In the formula, $\bar{g}_{\Lambda\eta}k$ represents the partial decay width of the $\Lambda\eta$ channel, where $\bar{g}_{\Lambda\eta}$ and k are the dimensionless coupling constant and the decay momentum in the $\Lambda\eta$ channel, respectively. Here, k becomes imaginary below the $\Lambda\eta$ threshold so as to keep the analytic continuity. We also note that for $\bar{g}_{\Lambda\eta} = 0$, Eq. (2) reduces to the BW function [Eq. (1)] with $m_f = m_0$ and $\Gamma' = \Gamma_0$.

Due to the scaling behavior of the Flatté function [27], we fix m_f when we perform a fit and repeat the fit with various m_f values [5]. The signal PDF, Flatté function, is convolved with

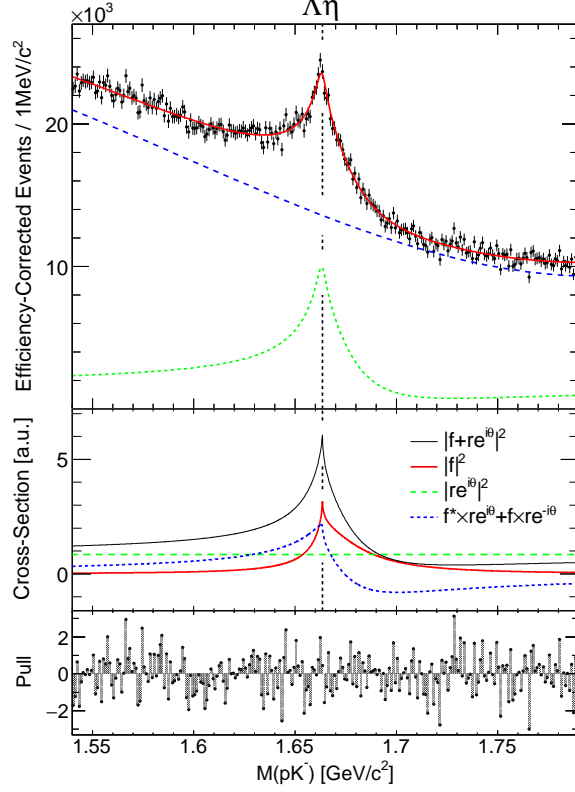


FIG. 5. Fit to the Λ_c^+ yield in $M(pK^-)$ spectrum with Flatté model to which a complex constant is added coherently with $m_f = 1674.4$ MeV/ c^2 and $\theta = \pi$ being fixed. In the upper panel, the curves indicate the full fit model (solid red), Flatté function with complex constant added coherently (dashed green), and incoherent background Λ_c^+ decay events (long-dashed blue). The middle panel shows the breakdown for $|f + re^{i\theta}|^2$; the curves indicate the full function (thin solid black), $|f|^2$ (thick solid red), $|re^{i\theta}|^2$ (long dashed green), and the interference term (dashed blue). The detector response is not taken into account. The bottom panel shows the pull distribution of the fit.

the double-Gaussian function for detector responses and a fifth-order Chebyshev polynomial represents background Λ_c^+ decay events. Figure 3(a) shows the results on $\bar{g}_{\Lambda\eta}$ and χ^2 for each fixed m_f . Strong correlation between $\bar{g}_{\Lambda\eta}$ and m_f is seen as expected from the scaling. Typical fit results with fixed $m_f = 1662.9$ MeV/ c^2 and 1674.4 MeV/ c^2 are shown in Fig. 4.

The best fit is obtained by taking into account an interference with another S -wave amplitude such as a tail of $\Lambda(1405)$. We take a constant, $re^{i\theta}$, as the amplitude for these Λ_c^+ events, and add it to the Flatté coherently; here, θ is simply fixed to π to represent the Λ_c^+ events distribution, which drops rapidly above the $\Lambda\eta$ threshold, and variations from the

fixed θ are considered as a source of systematic uncertainty.

We perform a binned least- χ^2 fit with the combined function, $\frac{dN}{dm} \propto |f(m) + re^{i\theta}|^2$, by changing the fixed m_f . Incoherent background Λ_c^+ decay events are represented by a third-order Chebyshev polynomial. As shown in Fig. 3(b), a strong correlation between m_f and $\bar{g}_{\Lambda\eta}$ is still seen even when the interference is taken into account. The best fit with $\chi^2/\text{ndf} = 1.06$ (257/243) is obtained at $m_f = 1674.4 \text{ MeV}/c^2$, and the result is shown in Fig. 5. Γ' and $\bar{g}_{\Lambda\eta}$ are determined to be $27.2 \pm 1.9 \text{ MeV}$ and 0.258 ± 0.023 , respectively, where the uncertainties are only statistical. The partial width, $\Gamma_{\Lambda\eta}$, of $\Lambda\eta$ channel is calculated as the product of $\bar{g}_{\Lambda\eta}$ and $q_{\Lambda\eta}^0$, which is the center-of-mass momentum of $\Lambda\eta$ at $m = m_f$. Then, the total width, Γ_{tot} , defined as a sum of Γ' and $\Gamma_{\Lambda\eta}$ is obtained to be $50.3 \pm 2.9 \text{ MeV}$, where the uncertainty is only statistical.

TABLE I. Systematic uncertainties in Γ' , $\bar{g}_{\Lambda\eta}$, and Γ_{tot} from Flatté fit for the pK^- peak structure.

Source	Γ' (MeV)	$\bar{g}_{\Lambda\eta}$ ($\times 10^{-3}$)	Γ_{tot} (MeV)
Bin size	± 0.0	± 3	± 0.3
Detector resolution	$+0.3, -0.4$	$+7, -6$	± 0.2
Absolute mass scale	± 0.8	$+5, -6$	± 1.3
Fit range	$+1.1$	-36	$+0.8, -2.4$
Efficiency correction	± 0.6	± 8	± 0.2
PDF model	$+3.5, -1.9$	$+9, -29$	$+3.4, -2.1$
θ	± 3.3	± 59	± 2.0
Total	$+5.0, -3.9$	$+61, -75$	$+4.2, -4.0$

We estimate the systematic uncertainties for $\bar{g}_{\Lambda\eta}$ and Γ' of the Flatté model with a constant added coherently. These systematic uncertainties are listed in Table I. We change the bin size of the $M(pK^-)$ distribution to 2 MeV to check the effect of binning. Systematic uncertainty from the mass resolution is estimated by increasing or decreasing the mass resolution by 20%. The effect of the absolute mass scaling is estimated by shifting the overall $M(pK^-)$ distribution by $\pm 0.2 \text{ MeV}/c^2$, which is a difference between a measured Λ_c^+ mass and the world-average value [28].

We vary the fit range to estimate the systematic uncertainty from the choice of the

fit range. The same PDFs are used for fitting to a narrow range from 1.55 GeV/ c^2 to 1.78 GeV/ c^2 . In the wide fit range from 1.48 GeV/ c^2 to 1.8 GeV/ c^2 , the peak structure of $\Lambda(1520)$ appears and is represented by a D -wave relativistic BW function convolved with a double Gaussian function to represent detector responses. Background Λ_c^+ events are represented by a seventh-order Chebyshev polynomial. The largest differences in the fit results are considered as the systematic uncertainty from the fit range. A systematic uncertainty from the efficiency correction is estimated by performing a fit to the $M(pK^-)$ distribution without the efficiency correction.

To estimate a systematic uncertainty due to the PDF modelling, we perform the fit with various PDFs. The PDF for the incoherent Λ_c^+ decay events is changed to second and fourth-order Chebyshev polynomials. We also change the non-relativistic Flatté function to a relativistic form. In addition, we study a case where all the background Λ_c^+ decay events are coherent. The total PDF is changed to $|f(m) + \sqrt{(p_0 + p_1m + p_2m^2 + p_3m^3)}e^{i\theta}|^2$, where p_i s ($i = 0, 1, 2$, and 3) and θ are free parameters. The largest differences in the fit results of the PDF models are taken as the systematic uncertainty from the PDF model.

In the Flatté fit, the reduced χ^2 is improved when the interference term is added, as it reproduces the drop of the background level around the peak structure. It indicates a significant interference with the background S -wave amplitude. Here we note that resonances in higher partial waves would not affect the cusp shape, because the discontinuity in the higher partial waves appear only in the second or higher derivatives, and the interference with S -wave vanishes with an integral over solid angle. The value of m_f that gives the best χ^2 is 1674.4 MeV/ c^2 , which is consistent with the recent measurement of $\Lambda(1670)$ mass, $1674.3 \pm 0.8 \pm 4.9$ MeV/ c^2 [29]. The total width at $m_f = 1674.4$ MeV/ c^2 is estimated as $50.3 \pm 2.9^{+4.2}_{-4.0}$ MeV and is also consistent with the recent measurement, $36.1 \pm 2.4 \pm 4.8$ MeV, within 1.9σ of the total uncertainty. In order to determine partial widths of $\Lambda\eta$ and pK^- and the Flatté parameters more accurately, a simultaneous-fit analysis with the $\Lambda(1670)$ peak structure in the $\Lambda\eta$ distribution is required.

The fit result with the Flatté function to which the constant is coherently added shows the best reduced χ^2 of 1.06 (257/243, $p = 0.25$), in contrast to 1.27 (308/243, $p = 3.1 \times 10^{-3}$) from the best BW fit. In particular, the Flatté function reproduces the shape near the peak point better than the BW function. These results show that the present peaking structure is explained better by a threshold cusp than to a new hadron resonance by more than 7σ .

This gives the first identification of a threshold cusp in hadrons from the spectrum shape. In the cusp interpretation, the structure near the $\Lambda\eta$ threshold is explained without the need of a new resonance. We also note that LHCb explained the structure using a BW function with fixed mass and width [13]. A small deviation is observed near the peak structure, but not considered as significant.

We thank the KEKB group for the excellent operation of the accelerator, and the KEK cryogenics group for the efficient operation of the solenoid.

-
- [1] S.-K. Choi *et al.* (Belle Collaboration), Observation of a Narrow Charmoniumlike State in Exclusive $B^\pm \rightarrow K^\pm \pi^+ \pi^- J/\psi$ Decays, Phys. Rev. Lett. **91**, 262001 (2003).
 - [2] R. Aaij *et al.* (LHCb Collaboration), Observation of $J/\psi p$ Resonances Consistent with Pentaquark States in $\Lambda_b^0 \rightarrow J/\psi K^- p$ Decays, Phys. Rev. Lett. **115**, 072001 (2015).
 - [3] R. Aaij *et al.* (LHCb Collaboration), Observation of a Narrow Pentaquark State, $P_c(4312)^+$, and of the Two-Peak Structure of the $P_c(4450)^+$, Phys. Rev. Lett. **122**, 222001 (2019).
 - [4] E. P. Wigner, On the behavior of cross sections near thresholds, Phys. Rev. **73**, 1002 (1948).
 - [5] R. Aaij *et al.* (LHCb Collaboration), Study of the lineshape of the $\chi_{c1}(3872)$ state, Phys. Rev. D **102**, 092005 (2020).
 - [6] J. Batley *et al.* (NA48/2 Collaboration), Observation of a cusp-like structure in the $\pi^0\pi^0$ invariant mass distribution from $K^\pm \rightarrow \pi^\pm \pi^0 \pi^0$ decay and determination of the $\pi\pi$ scattering lengths, Phys. Lett. B **633**, 173 (2006).
 - [7] J. Batley *et al.* (NA48/2 Collaboration), Determination of the S-wave $\pi\pi$ scattering lengths from a study of $K^\pm \rightarrow \pi^\pm \pi^0 \pi^0$ decays, Eur. Phys. J. C **64**, 589 (2009).
 - [8] V. L. Kashevarov *et al.* (A2 Collaboration at MAMI), Study of η and η' Photoproduction at MAMI, Phys. Rev. Lett. **118**, 212001 (2017).
 - [9] S. Acharya *et al.* (A Large Ion Collider Experiment Collaboration), Scattering Studies with Low-Energy Kaon-Proton Femtoscopy in Proton-Proton Collisions at the LHC, Phys. Rev. Lett. **124**, 092301 (2020).
 - [10] F. Afzal *et al.* (CBELSA/TAPS Collaboration), Observation of the $p\eta'$ Cusp in the New Precise Beam Asymmetry Σ Data for $\gamma p \rightarrow p\eta$, Phys. Rev. Lett. **125**, 152002 (2020).
 - [11] Unless stated otherwise, charge-conjugate modes are implied throughout this Letter.

- [12] S. B. Yang *et al.* (Belle Collaboration), First Observation of the Doubly Cabibbo-Suppressed Decay of a Charmed Baryon: $\Lambda_c^+ \rightarrow pK^+\pi^-$, Phys. Rev. Lett. **117**, 011801 (2016).
- [13] (LHCb Collaboration), Amplitude analysis of the $\Lambda_c^+ \rightarrow pK^-\pi^+$ decay and Λ_c^+ baryon polarization measurement, arXiv:2208.03262.
- [14] B.-C. Liu and J.-J. Xie, The $K^-p \rightarrow \eta\Lambda$ reaction in an effective Lagrangian model, Phys. Rev. C **85**, 038201 (2012).
- [15] H. Kamano, S. X. Nakamura, T.-S. H. Lee, and T. Sato, Dynamical coupled-channels model of K^-p reactions. II. Extraction of Λ^* and Σ^* hyperon resonances, Phys. Rev. C **92**, 025205 (2015).
- [16] A. Starostin *et al.* (The Crystal Ball Collaboration), Measurement of $K^-p \rightarrow \eta\Lambda$ near threshold, Phys. Rev. C **64**, 055205 (2001).
- [17] S. Kurokawa and E. Kikutani, Overview of the KEKB accelerators, Nucl. Instrum. Methods Phys. Res., Sect. A **499**, 1 (2003), and other papers included in this volume; T. Abe *et al.*, Achievements of KEKB, Prog. Theor. Exp. Phys. **2013**, 03A001 (2013), and references therein.
- [18] Z. Natkaniec *et al.* (Belle SVD2 Group), Status of the Belle silicon vertex detector, Nucl. Instrum. Methods Phys. Res., Sect. A **560**, 1 (2006); Y. Ushiroda (Belle SVD2 Group), Belle silicon vertex detectors, Nucl. Instrum. Methods Phys. Res., Sect. A **511**, 6 (2003).
- [19] A. Abashian *et al.* (Belle Collaboration), The Belle detector, Nucl. Instrum. Methods Phys. Res., Sect. A **479**, 117 (2002); also see detector section in J. Brodzicka *et al.* (Belle Collaboration), Physics achievements from the Belle experiment, Prog. Theor. Exp. Phys. **2012**, 04D001 (2012).
- [20] T. Sjöstrand, S. Mrenna, and P. Skands, PYTHIA 6.4 physics and manual, J. High Energy Phys. **2006** (05), 026.
- [21] J. Lange, The EvtGen particle decay simulation package, Nucl. Instrum. Methods Phys. Res., Sect. A **462**, 152 (2001); T. Sjöstrand, P. Edén, C. Friberg, L. Lönnblad, G. Miu, S. Mrenna, and E. Norrbin, High-energy-physics event generation with Pythia 6.1, Comput. Phys. Commun. **135**, 238 (2001).
- [22] R. Brun *et al.*, GEANT 3 Users Guide, CERN Report No. DD/EE/84-1, 1984.
- [23] E. Nakano, Belle PID, Nucl. Instrum. Methods Phys. Res., Sect. A **494**, 402 (2002).

- [24] K. Hanagaki, H. Kakuno, H. Ikeda, T. Iijima, and T. Tsukamoto, Electron identification in Belle, Nucl. Instrum. Methods Phys. Res., Sect. A **485**, 490 (2002).
- [25] In equation, here and below, we use a natural unit that c equals to 1.
- [26] S. M. Flatte, Coupled-channel analysis of the $\pi\eta$ and KK systems near KK threshold, Phys. Lett. B **63**, 224 (1976).
- [27] V. Baru, J. Haidenbauer, C. Hanhart, A. Kudryavtsev, and U.-G. Meißner, Flatté-like distributions and the $a_0(980)/f_0(980)$ mesons, Eur. Phys. J. A **23**, 523 (2005).
- [28] P. Zyla *et al.* (Particle Data Group), Review of Particle Physics, Prog. Theor. Exp. Phys. **2020**, 083C01 (2020).
- [29] J. Y. Lee *et al.* (Belle Collaboration), Measurement of branching fractions of $\Lambda_c^+ \rightarrow \eta\Lambda\pi^+$, $\eta\Sigma^0\pi^+$, $\Lambda(1670)\pi^+$, and $\eta\Sigma(1385)^+$, Phys. Rev. D **103**, 052005 (2021).